



УДК 551.463.2:547.211

Yu.G. Artemov, research scientist, **V.N. Egorov**, correspondent member of NAS Ukraine,
G.G. Polikarpov, academician NAS Ukraine, **S.B. Gulin**, DSc, chief scientist

A. O. Kovalevsky Institute of Biology of the Southern Seas, National Academy of Sciences of Ukraine,
Sevastopol, Ukraine

METHANE EMISSION TO THE HYDRO- AND ATMOSPHERE BY GAS BUBBLE STREAMS IN THE DNIEPER PALEO-DELTA, THE BLACK SEA

To estimate methane flux from natural gas bubble streams (seepages) a combined approach was applied, inclusive of detailed echo survey of investigated area and data analysis with the use of specialized software, GIS technique and mathematic simulation. A precise location map of methane seepages in the Dnieper paleo-delta region was obtained. In total 2200 seepages were identified at the investigated area of 387.1 km², which release 16.74 10⁶ m³ at atmospheric pressure (STP), or 12.0 10⁻³ teragram (Tg) methane a year. Statistical distribution of individual seepage methane flux rates conforms to the lognormal law. We found that 1.9% of methane from gas bubble streams reaches the atmosphere in gas phase, while 98.1% dissolves in the water column. Thus, the most part of methane remains in sea water and enters into physical, chemical and biological transformation processes of carbon-containing compounds.

Keywords: gas bubble streams, methane flux, Dnieper paleo-delta, Black Sea

Over the last decades it becomes clearly evident that emanations of gas bubble streams from the sea floor (gas seeps) are widespread at the ocean shelf and continental slope [8, 22, 23, 33, 44, 51, 38, 68]. Only recently the attention was attracted to this phenomenon as a potential source of atmospheric methane [21, 31, 34, 39]. After carbon dioxide, methane is considered to be the most important green-house gas, which content in the atmosphere increases by 0.5 – 1% a year and doubled during the last century [54]. It is supposed at present that annual methane intake to the atmosphere ranges from 535 to 598 Tg (1 Tg = 10¹² g) of which 360 – 430 Tg have an anthropogenic origin, while 160 – 240 Tg come from natural sources, including marine gas seeps [32, 36, 52]. At that time, known estimates of the total emission rate for atmospheric methane from gas seeps vary by orders of magnitude: 0.5 – 1.9 [21], 10–30 [41], 65–146 Tg/yr [34]. Such a wide value scatter is rather inherent to these estimations as they are obtained by extrapolation from a few particular ob-

servations and objective complexities are met when determining factors, which have an influence on methane evasion from the seabed and methane consumption in the water column [55]. It is believed that the ecological role of methane seeps could be understood better at the cost of increasing the factual data pool representing the local and regional features of seepage manifestations, such as: number, spatial distribution and dimensions of gas outlets, the relation between the sea-floor morphology and seep occurrences, intensity of ebullition from the sea floor, physical-chemical characteristics of bubbles in gas plumes and others. Earlier the rate of atmospheric methane emission from marine seeps has been documented for very limited regions, mainly shallower than 50 – 70 m: in southern California on shelf of northern Santa Barbara Channel [18, 31, 64], on the UK continental shelf [38] and in the offshore area of Bulgarian Black Sea Zone [25].

According to long-term acoustic observations carried out by scientists from IBSS NASU

on board the R/V “Professor Vodyanitskiy”, gas bubble streams in the Black Sea are generally occurred at river mouth areas, the edge of the shelf, the continental slope and also associated with mud volcanism [3]. One of the most active seepage areas in the Black Sea is the Dnieper paleo-delta where the large number of venting site manifestations have been recognized (Inset Fig. 1).

The discovery of gas bubble streams at this area, which came out from results of the R/V “Professor Vodyanitskiy” 28th cruise, was reported for the first time in 1989 [6]. Later on, the Dnieper paleo-delta stood a survey area for numerous multidisciplinary investigations targeted the gas bubble streams phenomenon, such as: analysis of localization, spatial distribution and environmental role of methane seeps [0, 2, 3, 7, 8, 11, 13, 26]; study of geological conditions for gas deposit generation [10, 11, 49]; studying the mechanism of

bacterial oxidation of methane and formation of carbonate build-ups in anoxic waters [4, 9, 37, 45, 48]; determination of the age and genesis of methane in the Black Sea [5, 29, 30]. The aim of the present work is to quantify the emission of gaseous methane to the water column and atmosphere at this area of the Black Sea. Statistical data on individual methane flux rates from seepages are presented.

Materials and methods. Our work is based on data acquired during the detailed acoustic survey in the north-western Black Sea on board the R/V « Professor Vodyanitskiy» in 58th (May – June 2003) and 60th (May – June 2004) cruises under the framework of the EU project «ContRi-bution of high-Intensity gas seeps in the Black Sea to Methane Emission to the Atmosphere (CRI-MEA)» (Fig. 1).

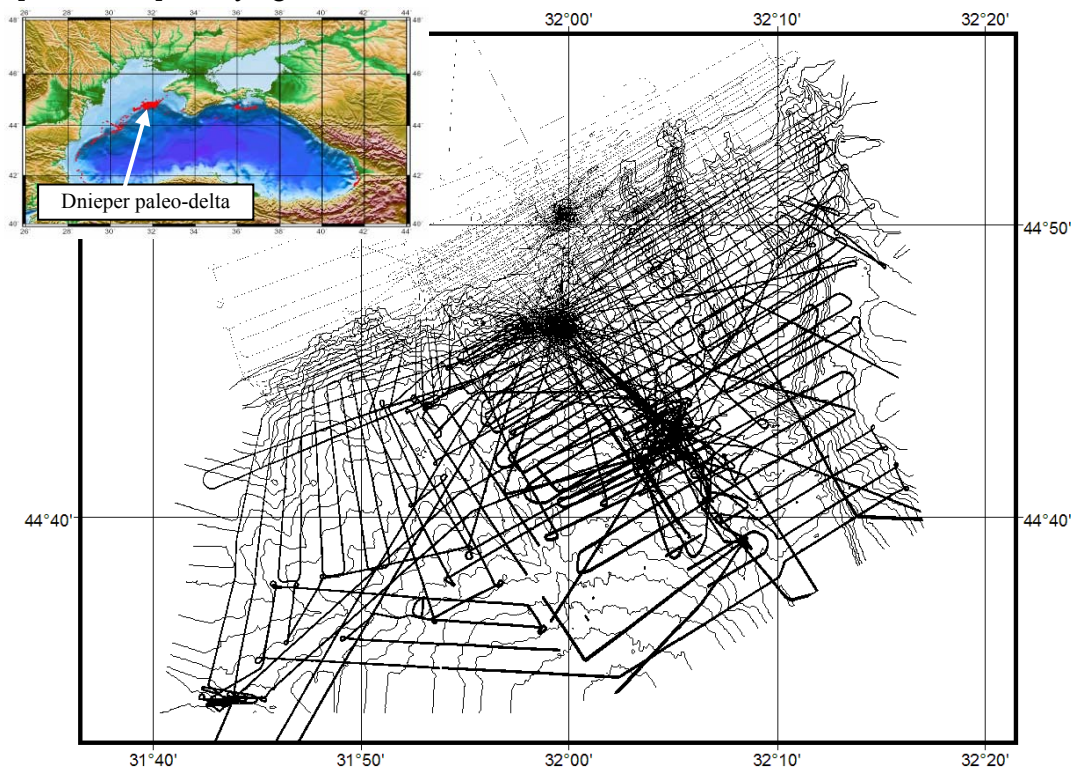


Fig. 1 Ship’s track in the study area. Inset shows location map of gas seeps in the Black Sea according to long-term acoustic observations carried out by scientists from IBSS NASU on board the R/V “Professor Vodyanitskiy” [3]. Active seepage areas are represented by red dots

Рис. 1 Маршрут судна в районе работ. На врезке: карта распределения струйных метановых газовыделений в Черном море по данным многолетнего мониторинга на НИС «Профессор Водяницкий» [3]. Участки выхода газа отмечены красными точками

It is well known that the echosounding observation of the water column is a convenient and efficient method for the detection of bubble releases from the sea-floor [7, 24, 47]. Echo responses from numerous gas bubbles, rising towards the sea surface, combine on echograms into vertically elongated figures, which shape resembles flares. This analogy is especially vivid if ap-

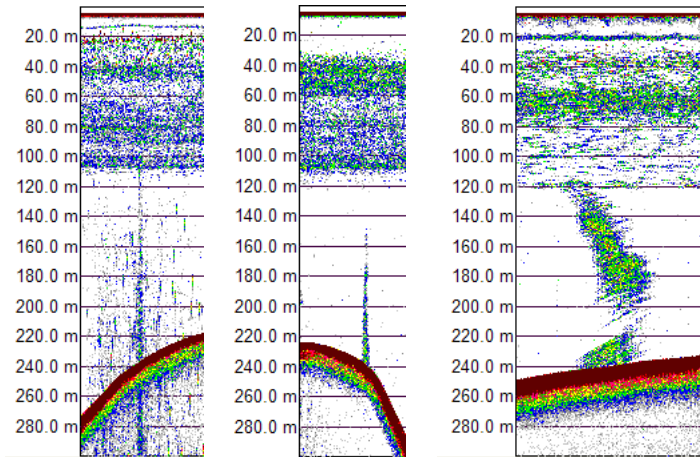


Fig. 2 Echograms of the gas flare from seep site at 240 m water depth

Рис. 2 Эхограммы факелов струйного газоразделения на глубине 240 м

In fact, each an acoustic flare represents a particular realization of the echo-signal forming process, which is stochastic by nature and subjected to various factors, such as: backscattering properties of gas bubbles, sonar characteristics and settings, ship speed and travel direction. Among other factors, we focused our attention on those which arise from the character of the spatial distri-

bution of seeps in the investigated area. From underwater observations with the use of TV submersible vehicle MiniRover MK-II [26], scientific submarine “Benthos-300” [9] and the submersible “Jago” [48] it was noted that the typical gas outlet is a relatively small (from a tenth of a square centimeter to meters), spatially separated from another seeps area on the sea floor (Fig. 3).



Fig. 3 Methane-rich gas discharge in anoxic waters of the Black Sea providing formation and growth of carbonate build-up. Still photograph was taken from the porthole of scientific submarine “Benthos-300”. Visibility range is limited by the area of projector light spot $\approx 100 \text{ m}^2$ [9]

Рис. 3 Выход метана в сероводородной зоне Черного моря, обеспечивший образование и рост бактериальной постройки. Снимок сделан из иллюминатора исследовательской подводной лодки «Бентос». Зона видимости ограничена площадью светового пятна прожектора $\approx 100 \text{ м}^2$ [9]

These observations conform to our acoustic data which indicate that echo returns come in most cases from the only one flare at a time, i.e. the spatial resolution of a gas flare takes place (Fig. 4).

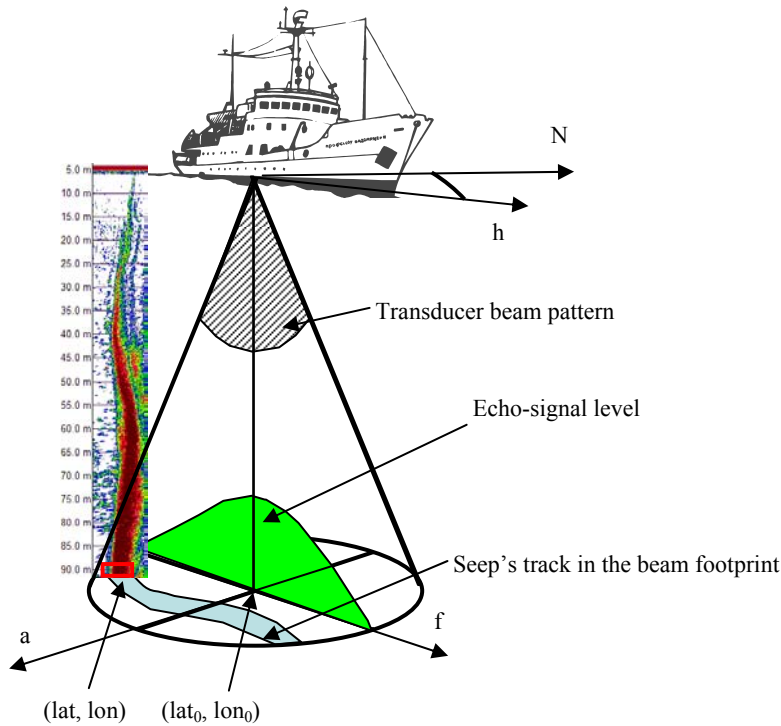


Fig. 4 Schematic showing acoustic detection of spatially resolved flare. h – direction of vessel travel (heading), N – north direction, lat_0, lon_0 – geographic coordinates of the beam axis, lat, lon – actual seep location, a, f – angular deflection of the flare from the beam axis athwartships and alongship, correspondingly

Рис. 4 Схема акустического детектирования пространственно разрешенного факела. h – курс судна, N – направление на север, lat_0, lon_0 – географические координаты центра звукового луча, lat, lon – действительные координаты сипа, a, f – углы направления на факел, отсчитываемые от центра антенны поперек и вдоль судна, соответственно

As shown in Fig. 4, when the single seepage is crossing the sound beam, it should be expected at any given instance that: a) the echo-signal level (figure in green) depends on the angular deflection of the flare from the beam axis due to the beam pattern (hatched figure); b) even if the flare is distinctly recognized in the echogram, the real geographical location of the seepage can differ from that of beam axis (seep's track in the beam footprint is highlighted by the figure in blue). Any reasoning in this paragraph concerns thin bottom layer marked in echogram Fig. 4 by red rectangle.

Indeed, the echo level from a single acoustic target, positioned in the insonified volume, is described by the equation [59]:

$$P_r = P_t G(a, f) \frac{10^{-\alpha r}}{4\pi r^2} \sigma_{bs} \frac{10^{-\alpha r}}{4\pi r^2} \frac{\lambda^2}{4\pi} G(a, f), \quad (1)$$

where P_t and P_r are the transmitted and received power, correspondingly, σ_{bs} is the effective backscattering cross-section area of the target,

$G(a, f)$ is the transducer gain towards the target as the function of angular deflection from the acoustic axis athwartships and alongship, correspondingly, r is the transducer-target range, α is the sound attenuation constant, and λ is the sound wavelength.

Denoting $K = P_t \left(\frac{10^{-\alpha r}}{4\pi r^2} \right)^2 \frac{\lambda^2}{4\pi}$, equation

(1) can be rewritten in a compact form

$$P_r = K G^2(a, f) \sigma_{bs} \quad (2)$$

As direct signal is a sound pulse, the whole insonified volume dV contributes to the echo-signal at any particular instance [59]:

$$P_r = K \int_V G^2(a, f) s_v dV, \quad (3)$$

where dV is assumed to consist of small elementary volumes ∂V , s_v is the volume backscattering coefficient defined as the backscattering area of contained in the elementary volume targets per this volume, i.e. $s_v = \partial \sigma_{bs} / \partial V$, a and f specify the direction from the transducer face to the elementary volume ∂V .

On the assumption that the cross-section of gas flare is small, at least at its “root”, it can be stated that $s_v = 0$ everywhere in the insinified volume of the thin bottom layer except for containing gas bubbles small volume ∂V where s_v is s_{vs} on average. Denoting the mean 2-way sensitivity of transducer within the volume ∂V , $\bar{G}^2(a_s, f_s)$, (3) can be transformed to:

$$P_r = K \bar{G}^2(a_s, f_s) s_{vs} \partial V \quad (4)$$

Value of $s_{vs} \partial V$, by definition, is combined from the effective backscattering cross-section areas of all acoustic targets containing in the volume ∂V . If these targets (gas bubbles in our case) are randomly and homogeneously distributed in ∂V then

$$s_{vs} \partial V = n \bar{\sigma}_{bs}, \quad (5)$$

where n and $\bar{\sigma}_{bs}$ – correspondingly, the number and the mean backscattering cross-section of bubbles contained in the insinified volume, therefore

$$P_r = K \bar{G}^2(a_s, f_s) n \bar{\sigma}_{bs}. \quad (6)$$

Equation (6) shows in explicit form, that the echo level from gas flare depends on the backscattering property of gas bubbles, $\bar{\sigma}_{bs}$, number of bubbles, n , and the flare position in the insinified volume relative to the acoustic axis, $\bar{G}^2(a_s, f_s)$. It should be noted, that equation (6) differs from that of the volume reverberation model, which is deduced, as well known, from the assumption that the whole pulse shell is filled by a large number of randomly distributed over the beam cross-section targets [61]. In this latter case dV in (3) is replaced by $1/2c \tau r^2 d\Omega$, where c – sound speed, τ – pulse duration and Ω – solid angle, while s_v is considered to be a constant and $\int_{4\pi} G^2(a, f) d\Omega$ is substituted by Ψ – the equivalent two-way beam width of the transducer, within which limits the sensitivity is by convention steady and equal to 1:

$$P_r = K \frac{c \tau}{2} r^2 \Psi s_v \quad (7)$$

Equation (7) is referred to as the theoretical background of the echo-integration method [17, 60], which is widely used in fish stock assessment researches. The central aspect of these researches relates to the volumetric fish density $\rho = N/V$, where N is the number of fish in the volume V . According to the linearity principle of fisheries acoustics [27], there is a simple relationship between the volume (\bar{s}_v) and point ($\bar{\sigma}_{bs}$) backscattering characteristics averaged over large time/space extent $\bar{s}_v = \rho \bar{\sigma}_{bs}$. A few applications of the echo integration technique for estimating methane emission over seep fields are also documented, e.g. [53].

In the present study we use a modified echo-integration method based on the combination of equations (6) and (7):

$$N \bar{\sigma}_{bs} = \frac{s_v r^2 \Psi}{\bar{G}^2(a_s, f_s)} \quad (8)$$

where s_v is equivalent to the volume backscattering coefficient in terms of (7), i.e. as if n bubbles from (6) would dispersed randomly and homogeneously over the whole pulse shell, and N is the number of bubbles per 1 m of the flare height.

The employment of (8) allows making an appraisal of the individual intensity of gas bubble streams and also resulted from their activity methane flux to the water column and atmosphere.

To achieve objectives of present study a comprehensive approach is required for data collection, processing and analysis. This approach includes some interrelated steps to be passed through.

1. Data collection. Acoustic observations were performed with the calibrated scientific echo-sounder EK-500 unit equipped with 2 hull-mounted transducers (split-beam 38 kHz, nominal beam width 6.7° at -3 dB level, and conventional 120 kHz, beam width 9.4°), precision transceivers, internal microcomputer, display and printing devices for representing echograms in the real-time mode, and digital data transfer channels. We treated the echo sounder as a source of raw

acoustic data (the envelope and the electric angles of split-beam phases) which were registered at the output of the high-speed 10 Mbit ETHERNET communication line and processed in the remote computer. Measurements were stored in a set of files: low depth resolution vertical profiles of the volume backscattering strength (maximum 700 samples) *.fq#, high depth resolution vertical profiles of the volume backscattering strength (maximum 5000 samples) *.fv#, phase angles of the electrical output signal from quadrants of the split-beam transducer (maximum 5000 samples) *.fb1 and the log file *.str containing the references to all received from the echo sounder telegrams as well as the readings from the satellite navigation system FURUNO GP-80, where * is the file set name and # denotes transducer number which takes on a value of 1 or 2 (1 – 38 kHz channel, 2 – 120 kHz channel). For the purpose of our investigation, the special data logging and processing software was developed [15].

2. Determining the number and location of observed seeps. First, the obtained data were represented in the form of echogram and examined visually for flare occurrences. Depending on the noise level and the echo-signal strength, to gain the reliability of seep identification the various tools were employed in the echogram window of the WaveLens program: adjustment of the window extent and vertical scale (depth range), tuning the minimal visible echo level, switching between different color palettes as well as TVG laws – $20\log R$ or $40\log R$, application of the interactive noise elimination procedure [15]. Then, those parts of the echogram, which provisionally recognized as flares, were exposed to the detailed analysis with the use of the full set of acquired data (Fig. 5).

Shown in Fig. 5 SV values are determined according to (7) with the threshold level of -55 dB.

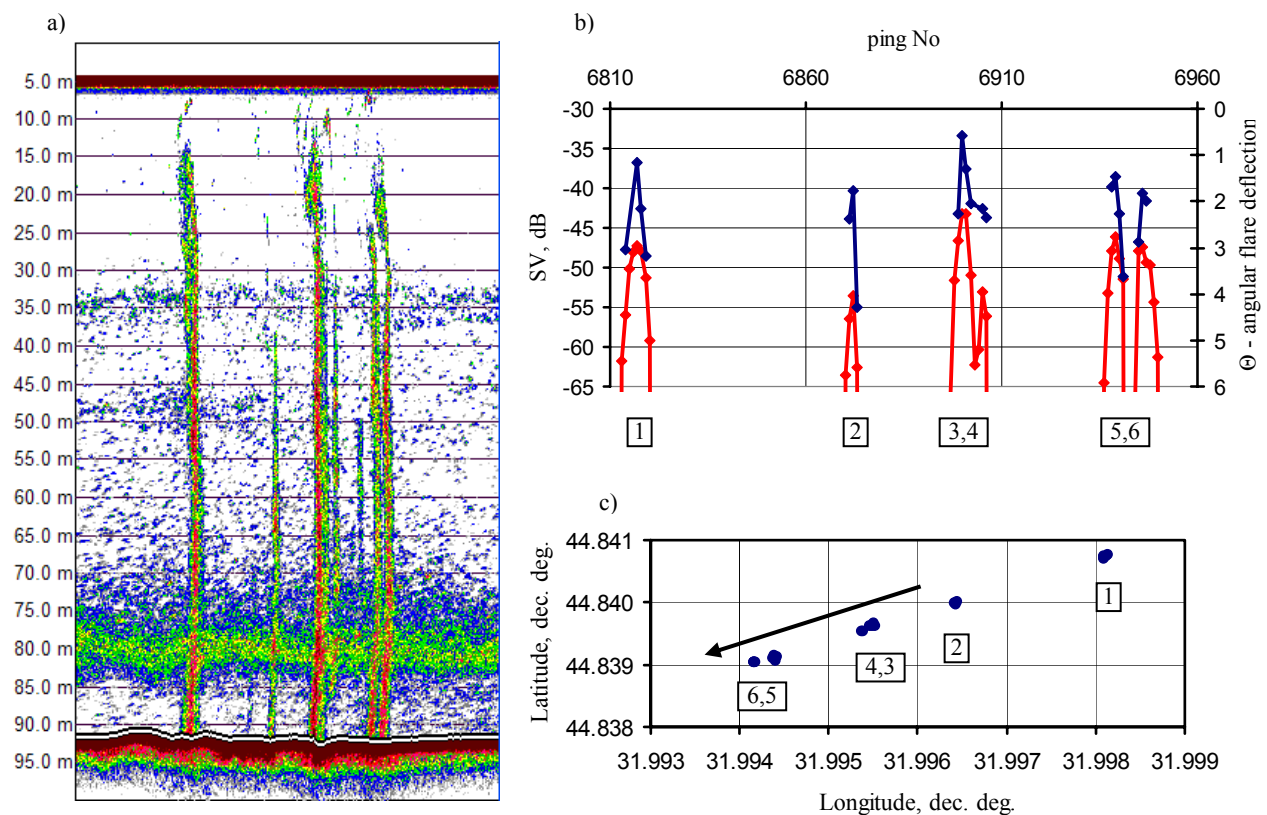


Fig. 5 Gas flare identification and determination of geographic coordinates of seepages: a) fragment of the echogram at 38 kHz with 0.3 ms pulse duration and 1 s ping rate. Vessel moved along the straight-line trajectory at a variable speed within the range of 4.6 – 5.7 knots. Detected flares are numbered 1 – 6; b) volume backscattering strength SV , dB (red line) and solid angular deflection of flares from the transducer axis Θ , degrees (blue line), averaged for each ping within 2 m near-bottom layer; c) geographical location of seeps 1 – 6. Ship's travel direction is indicated by the arrow.

Рис. 5 Обнаружение факелов и определение географических координат струйных газовыделений: а) фрагмент эхограммы, полученной при зондировании импульсами длительностью 0.3 мсек с частотой заполнения 38 кГц и периодом повторения 1 с. Судно двигалось прямолинейно с переменной скоростью в пределах 4.6 – 5.7 узла. Цифрами 1 – 6 отмечены обнаруженные газовые факелы; б) сила обратного объемного рассеяния SV , дБ (линии красного цвета) и угловое отклонение факелов от оси антенны Θ , градусы (синие линии), рассчитанные для каждой зондирующей посылки усреднением по придонному слою шириной 2 м; в) географическое положение сипов 1 – 6. Направление движение судна обозначено стрелкой.

It should be noted, that visual analysis of echograms was performed with low echo-signal threshold (in the order of -90 dB, TVG 20logR applied), efficient for detecting even weak flares at the periphery of the sound beam. However, when calculating SV the echo-signal threshold could be set to higher values to provide better spatial resolution for the seepage distinction as shown in Fig. 5.

The solid angle Θ , which represents the angular deflection of a flare from the beam axis, is calculated by formula:

$$\Theta = \arccos\left(\frac{1}{\sqrt{1 + \operatorname{tg}^2 a + \operatorname{tg}^2 f}}\right), \quad (9)$$

where a and f are flare angular deflection relative to the split-beam axis athwartships and alongship, correspondingly.

In Fig. 6 all Θ values of observed flares are drawn on the plot uniform quantile plot, from which it is seen that only in 10% cases flares were detected by the most sensible area of the transducer within 1° off the acoustic axes; while in 50% cases Θ exceeded the nominal half-width of the split-beam pattern (3.35°). As shown in Fig. 6, seeps, which angular deflection from the beam axis constituted no more than 6.5° , were distinguished in echograms with the probability of 97.5%. Because of this reason we assumed that the area, scanned during acoustic survey, coincides with the stripe along the ship's track which breadth refers to the 13° full-width sound beam footprint.

Depending on the direction to the insonified flare from the split-beam transducer face, the

small correction was introduced to GPS readings to determine the seep's position more precisely:

$$lat = lat0 + d * (\operatorname{tg}(f) * \cos(h) - \operatorname{tg}(a) * \sin(h)) / M \quad (10a)$$

$$= \quad + \quad +$$

$$(10b)$$

where $lat0$, $lon0$ and h – current GPS readings of the latitude, longitude and ship's heading, lat and lon are calculated seep position, d is water depth, M and N – the radius of curvature of the ellipsoid in the prime meridian and the radius of curvature of the ellipsoid in the prime vertical of the geodetic reference system WGS 84, correspondingly.

As illustrated in Fig. 5, any seep gets into the insonified volume for a short time period even at medium ship's speed (4 – 6 knots); so the possibility for obtaining representative statistical samples on a single traverse is very limited. However we used the consolidated data from various routes executed at different time, direction and speed. In total, more than 2000000 resulting echosounding pings insonifying one or another gas flare were made. The geoinformation system (GIS) ArcViewTM 3.3 was applied for data processing. When mapped on the GIS pad according to the georeference label (lat , lon), flare samples aggregated in a cluster indicating the seepage location. Number and coordinates of centers of such clusters were treated as quantity and localization characteristics of gas bubble streams in the investigated area (Fig. 7).

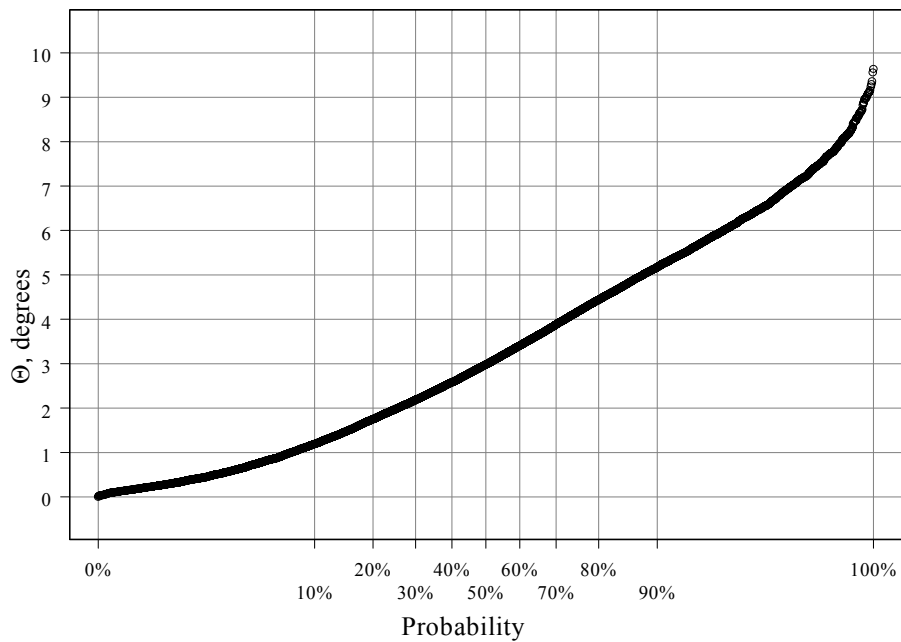


Fig. 6 Solid angles Θ of all detected flares showing on the uniform quantile plot

Рис. 6 Углы Θ обнаруженных эхо-откликов газовых факелов на графике квантилей равномерной функции распределения

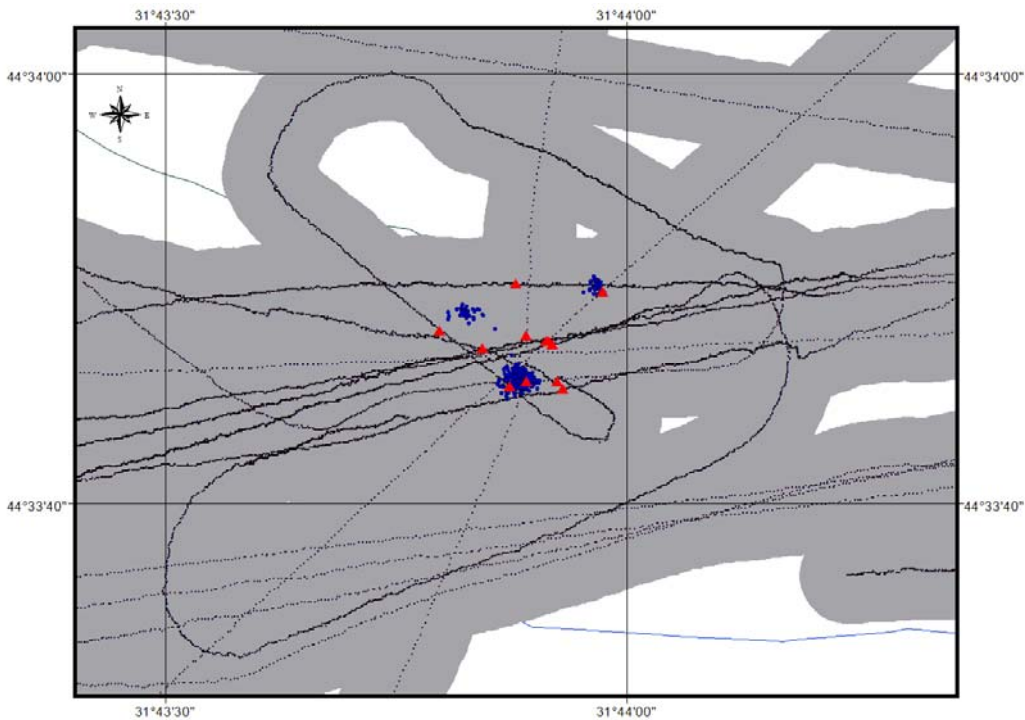


Fig. 7 Determining the actual number of seepages and their geographic locations. Notation used: – ship's track; – GPS readings (lat_0 , lon_0) for flares insonified at various traverse routes; – seepage routes; – seepage coordinates (lat , lon) calculated according to (10); – area of acoustic coverage calculated by ArcView™ as non-overlapping buffer zone around the ship's track which refers to the 13° full-width sound beam footprint.

Рис. 7 Определение

уточненных координат сипов. Обозначения: – маршрут судна; – координаты (lat_0 , lon_0), считанные с показаний GPS при пересечении факелами луча антенны эхолота на различных галсах судна; – координаты струйных газовыделений (lat , lon), вычисленные по формулам (10); – область акустического покрытия, рассчитанная ArcView™ как непересекающаяся буферная зона вокруг маршрута судна с учётом эффективной ширины диаграммы направленности антенны эхолота 13°.

3. Estimating the seep's productivity. As a measure of productivity the number of bubbles per 1 m flare height just above the sea floor (N in the equation 8) was used. It can be shown that N is proportionate to the frequency of bubble emitting from the sea floor. If Δt is the mean period of time between instants of bubble detachment from the sea floor and v_0 is the mean initial bubble rising speed, then the mean distance between bubbles in the lower part of gas flare constitutes $\Delta h = v_0 \Delta t$. Let N bubbles contain in water layer 1 m thickness above the seepage. Estimation of Δh can be expressed as $1/N$, therefore, $N = 1/v_0 \Delta t$.

The mean productivity of j -th seep \bar{N}_j was estimated by averaging over the corresponding cluster in the GIS pad according to (8):

$$\bar{N}_j = \frac{r^2 \Psi}{\sigma_{bs} m_j} \sum_{i=1}^{m_j} \frac{s_v^i}{G^2(a_s^i, f_s^i)}, \quad (11)$$

where i is the point number from a cluster and takes values from 1 to m_j .

The beam pattern factor $G^2(a, f)$ is a nominal characteristic of calibrated echo-sounders. For used in our study SIMRAD ES38B split-beam transducer it is expressed by formula [59]:

$$G^2(a, f) = 10^{-0.6((a/\varphi)^2 + (f/\psi)^2) - 0.18(a/\varphi)^2(f/\psi)^2} \quad (12)$$

where φ and ψ are half-width -3 dB beam angles athwartships and alongship, correspondingly.

Aiming to minimize the inaccuracy of formula (12) evaluation and to eliminate the influence of closely approximating seeps, only those points from a cluster were selected for averaging (11), which satisfy conditions $a_s^i \leq \varphi, f_s^i \leq \psi$.

Backscattering cross-sections of bubbles σ_{bs} were determined by direct split-beam measurements at flare "roots". These measurements require single bubbles to be spatially resolvable in the sampling volume; however we have found such a situation is rather atypical straight above seepage. Therefore, one of two generalized, instead of individual, $\bar{\sigma}_{bs}$ value was used in (11) depending on the seepage depth: one for depths ≤ 140 m, another – more than 140 m. The first value represents the statistical average of measurement results over many seeps at water depths 80 – 100 m, the second – 180 – 230 m. (Fig. 8).

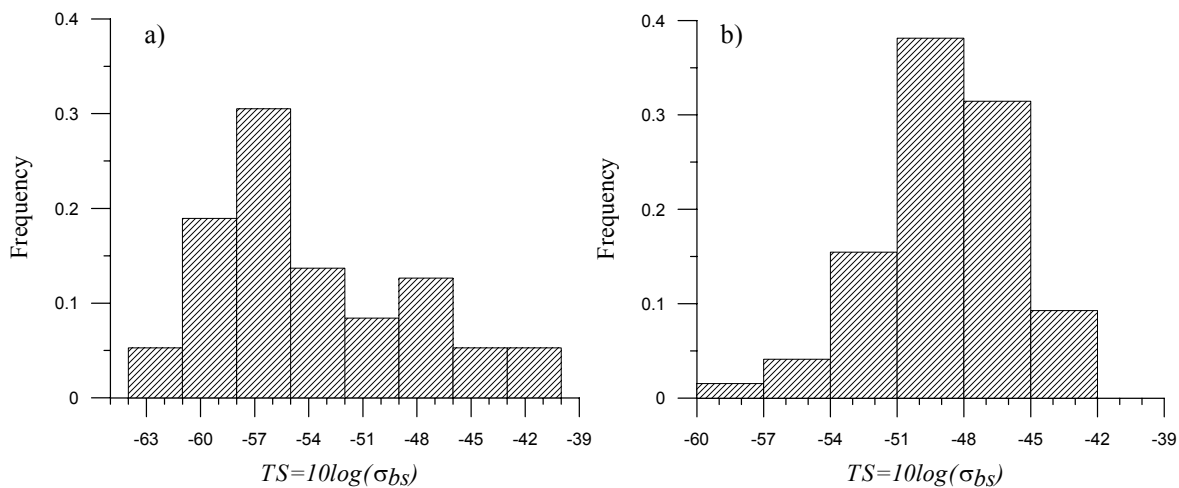


Fig. 8 The target strength $TS = 10 \log(\sigma_{bs})$ distribution bar charts of gas bubbles above the sea floor: a) at depths 80 – 100 m; b) at depths 180 – 230 m

Рис. 8 Гистограммы распределения силы цели $TS = 10 \log(\sigma_{bs})$ пузырьков над дном: а) на глубинах 80 – 100 м; б) 180 – 230 м

4. Evaluating the methane flux. We distinguished three constituents of the methane flux originated from gas bubble streams:

- initial upward flux Φ_0 , governing methane intake from the bottom to the water column;
- dispersed flux Φ_w , evolved from gas exchange between rising bubbles and surrounding water;
- flux to the atmosphere Φ_a , produced by bubbles reached the sea surface.

Our approach to flux calculations proceeds from the hypothesis that each flux constituent is linearly dependent on the seep productivity N (1/m):

$$\Phi_0 = N \cdot \bar{s}_0 \cdot \bar{m}_0 \quad (13)$$

$$\Phi_w = N \cdot \int_0^{H_0} \overline{s(h)} \cdot \frac{\partial \overline{m(h)}}{\partial h} \cdot dh \quad (14)$$

$$\Phi_a = \Phi_0 - \Phi_w = N \cdot (\bar{s}_0 \cdot \bar{m}_0 - \int_0^{H_0} \overline{s(h)} \cdot \frac{\partial \overline{m(h)}}{\partial h} \cdot dh) \quad (15)$$

where \bar{s}_0 is the mean initial bubble rising speed, \bar{m}_0 is the mean initial methane content in bubbles, $\overline{s(h)}$ is the mean bubble rising speed depending on depth, $\frac{\partial \overline{m(h)}}{\partial h}$ is the mean change of methane content in bubbles depending on depth, and H_0 is

Equations (13) – (15) refer to bubble parameters, namely the rising speed and the methane content at any depth throughout the entire water column, however measuring these parameters for each seep seems to be impractical. Meanwhile, after [20] gas bubble features are commonly considered in terms of two dynamic characteristics (both in cm/s) – the rise velocity v_b and the liquid-side rate of mass transfer across the surrounding bubble thin gas-liquid boundary layer k_b , which in turn depend on bubble size, shape, gas content and various environmental factors. At all that, the “clean” and the “dirty” bubble behavior modes are distinguished in [20], where “dirty” stands for various surfactants exist in sea water, such as: salts, polysaccharides, proteins, lipids [13]. As influence of surfactants on the bubble results in decreasing both v_b and k_b , we made few measurements of rising speed of seep bubbles to evaluate the validity of this factor in the Black Sea environment (Fig. 9).

These measurements were conducted over water depths of 90 – 650 m at different parts of gas flares (in near-bottom, pelagic, subsurface layers of the water column) using the single bubble track extraction technique incorporated into the WaveLens software [15].

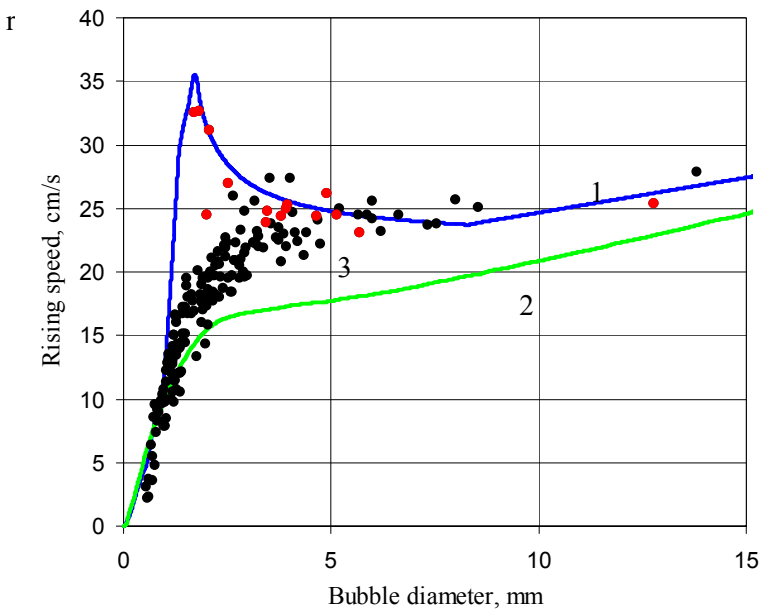


Fig. 9 Rising speed of bubbles in gas flares. 1 and 2 – theoretical curves for “clean” [50] and “dirty” [42] bubbles, correspondingly; 3 – data from our measurements (data for the flare “roots”, at the distance no more than 10 m from the sea floor, are indicated by red dots)
Рис. 9 Скорость подъема пузырьков в газовых факелах. 1 и 2 – теоретические зависимости для «чистых» [50] и «грязных» [42] пузырьков, соответственно; 3 - данные наших измерений (красными точками отмечены измерения в нижней части факелов, на расстоянии не более 10 м от дна)

As shown in Fig. 9, big bubbles of more than 5 mm in diameter can be considered as quite “clean”, while smaller bubbles, being initially “clean” in the lower part of a flare, adsorb surfactants during their ascent and gradually turn into “dirty” ones. This means that the state of a bubble at any instant depends on its full lifetime prehistory. From these considerations we estimated the lacking parameters in equations (13) – (15) by mathematical simulation. A model, based on the Van der Waals equation of state and the Fick’s law for diffusion, was developed for quantitative analysis of gas bubble behavior in the water column [16]. The major difference of our model from

others documented by various researchers [42, 46, 66, 67] concerns the algorithmic representation of bubble evolution from “clean” to “dirty” modes depending on the area of stagnant cap at the rear of rising bubble, where adsorbed surfactants accumulate due to the surface convection and cause the Marangoni effect [28, 43]. Analytic parameterizations for v_b (first proposed in [56]) and k_b were earlier successfully tested in experiments with air bubbles placed to tap water stream [14, 62, 63]. The “clean”, “transitional” and “dirty” modes of methane bubble behavior in the Black Sea environment calculated according to our model are illustrated in Fig. 10.

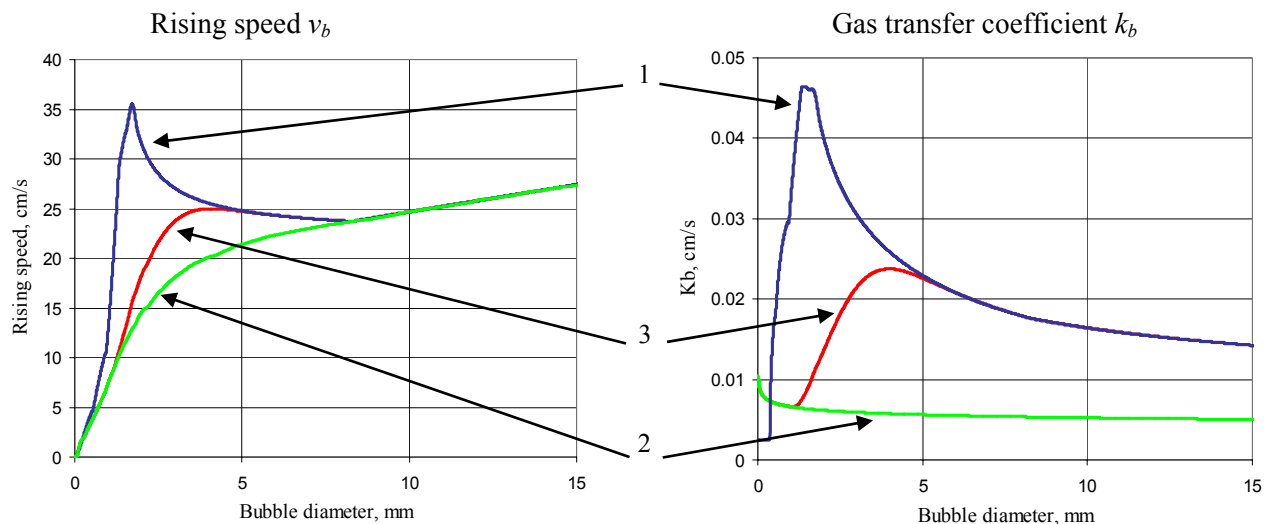


Fig. 10 Calculated values of v_b and k_b for three behavior modes of methane bubbles: 1 – “clean”; 2 – “dirty”; 3 – “transitional”

Рис. 10 Расчетные значения v_b и k_b , характеризующие три режима поведения пузырьков: 1 – «чистый»; 2 – «грязный»; 3 – «переходный»

The developed model was verified using time series data acquired by single bubble tracking observations (Fig. 11). Gas flares in whole were modeled as statistical ensembles of bubbles, which initial sizes were evaluated from measured back-scattering cross-sections σ_{bs} (Fig. 8, a, b) using the simplified formula [19]:

$$d = 2000 \sqrt{\sigma_{bs}}, \quad (15)$$

where d (mm) is bubble diameter.

Initial bubble sizes, calculated for shallow seeps, ranged from 1.3 to 18.3 mm with the mean of 5.1 mm, while for deep seeps, correspondingly, 2.0 – 15.7 mm with the mean of 7.7 mm. The obtained bubble size series were divided into 2-mm discrete classes and the bubble model was repeatedly executed for each size class. The model output included: time t , s; actual bubble depth h , m; bubble diameter d , mm; content of four gases in the bubble m , μmol . For shallow seeps (water depth ≤ 140 m) modeled bubbles were assumed to be

composed of CH₄, N₂, O₂ and Ar, while for seeps located at depths more than 140 m – of CH₄, N₂, He, Ar.

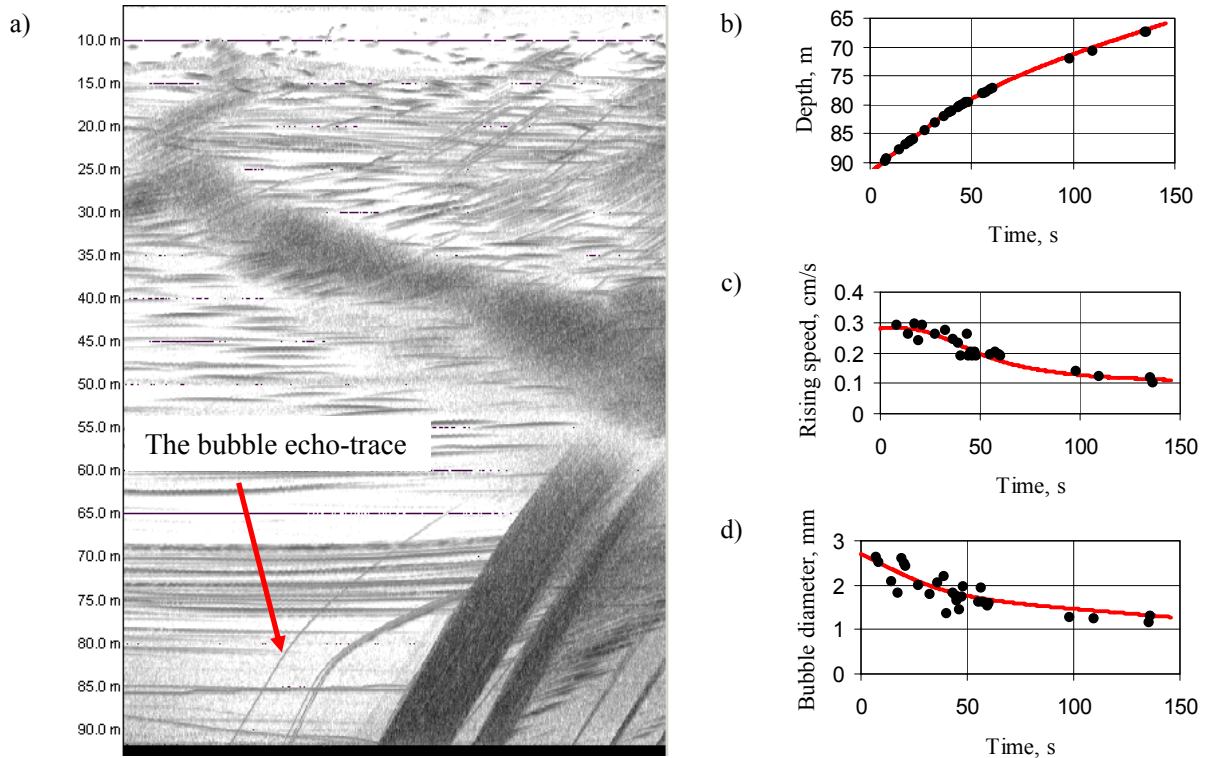


Fig. 11 Validation of methane bubble model results using acoustic observations for single bubbles: a) echogram with the echo-trace of single bubble; b) depth-time curve; c) change of rising speed; d) size transformation. In plots b), c) and d) points represent observed data; solid lines – model curves.

Рис. 11 Сопоставление акустических наблюдений и данных моделирования метанового пузырька: а) след одиночного пузырька на эхограмме; б) траектория в координатах глубина – время; в) изменение скорости подъема; д) изменение размеров. На рис б), с) и д) точками отмечены данные измерений, сплошные линии – модельные кривые.

In both cases the initial methane content was specified at 99% according to literature data [4, 5, 8, 48]. Model calculation stopped when bubble either reaches out the sea surface or decreases in size under 0.2 mm, what was interpreted as complete dissolution of a bubble. Then simulated for each size class data were used to compute the vertical profiles of methane content $m_m(h)$ and flux to the water column $f_m(h) = \frac{m_m(h + \Delta h) - m_m(h)}{\Delta t}$, where Δt is the bubble travel time through the depth interval of Δh . Finally, required for equations (13) – (15) the

statistical mean values of methane content and flux to the water column per 1 seep bubble were determined by the bubble size-frequency distribution weighted averaging over $m_m(h)$ - and $f_m(h)$ -profiles as illustrated in Fig. 12.

Results and discussion. During 2003 and 2004 CRIMEA cruises 55 Gbyte of acoustic data were collected in the research area, where 381.5 km² of the sea floor were covered by acoustic observations. In total, 2875 gas flares were detected from echograms. By data processing with the use of GIS technique it was determined that all observed flares belong to 2200 seeps located in dif

ferent water depths between 66.0 and 832.3 m (Fig. 13).

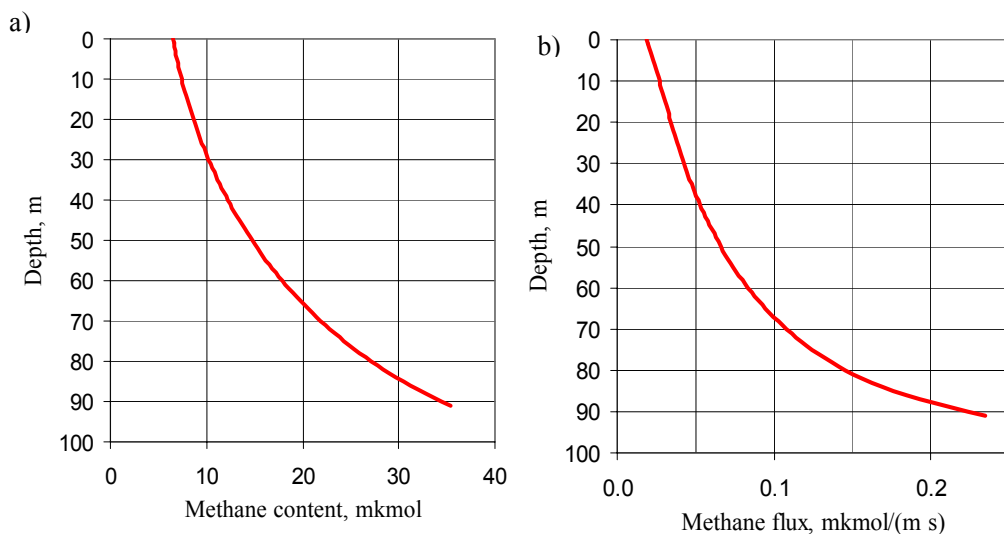


Fig. 12 Modeled vertical profiles of mean methane content $M(h)$ (a) and flux to the water column $F_w(h)$ (b) per 1 discharged bubble for a seepage located at 91.5 m depth

Рис. 12 Пример расчета вертикальных профилей содержания

метана $M(h)$ (а) и потока в водный столб $F_w(h)$ (б) для среднестатистического пузырька сипа, расположенного на глубине 91.5 м

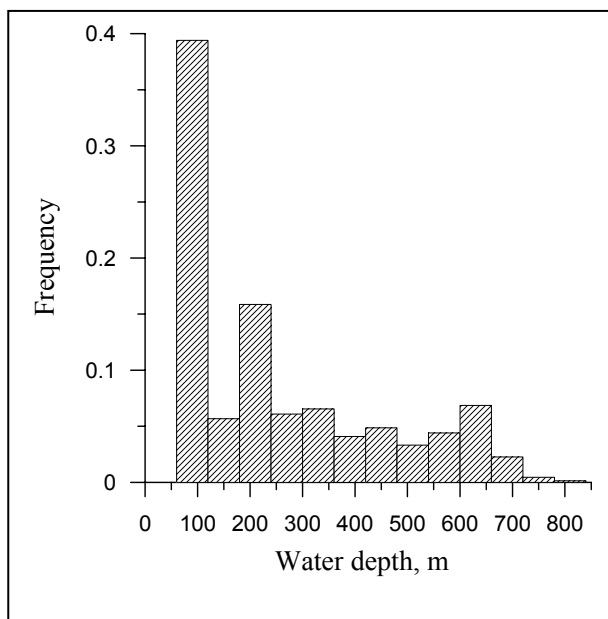


Fig. 13 Seep distribution versus depth in the investigated area

Рис. 13 Распределение сипов по глубине в районе исследований

Of the total amount of recognized seeps, the productivity N was determined for 811 seeps, well spatially resolved by the echosounder. The initial methane flux was estimated separately for seepage areas above and below the horizon of 140 m, corresponding, approximately, to the oxic-anoxic boundary in the Black Sea. Shown in Fig. 12 are frequency diagrams of initial methane fluxes from individual seeps Φ_0 (l/min STP), calculated for shallow and deep areas according to equation (14).

Normal quantile plots (Fig. 15) for log-transformed Φ_0 values testify that the statistical distribution of initial methane seep fluxes follows the log-normal law independently of seep location depths.

Presented in Fig. 15 data confirm to early proposed assumption that the log-normal distribution is applicable when methane flux over seepage areas is estimated by extrapolation of small amount of observations [65].

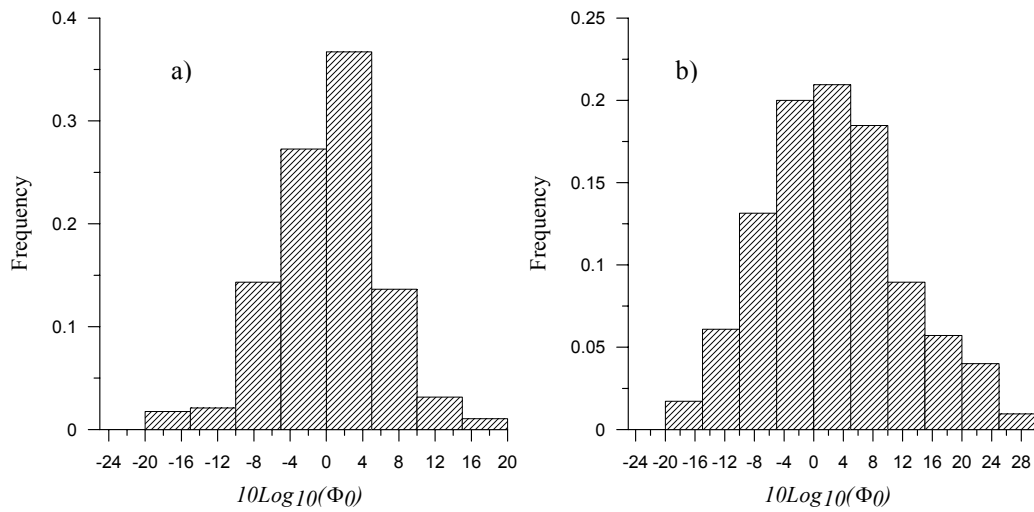


Fig. 14 Frequency distribution of initial methane fluxes from individual seeps in shelf (a) and deep (b) sectors of investigated area

Рис. 14 Частотные распределения индивидуальных начальных потоков сипов в шельфовом (а) и глубоководном (б) участках исследованного района

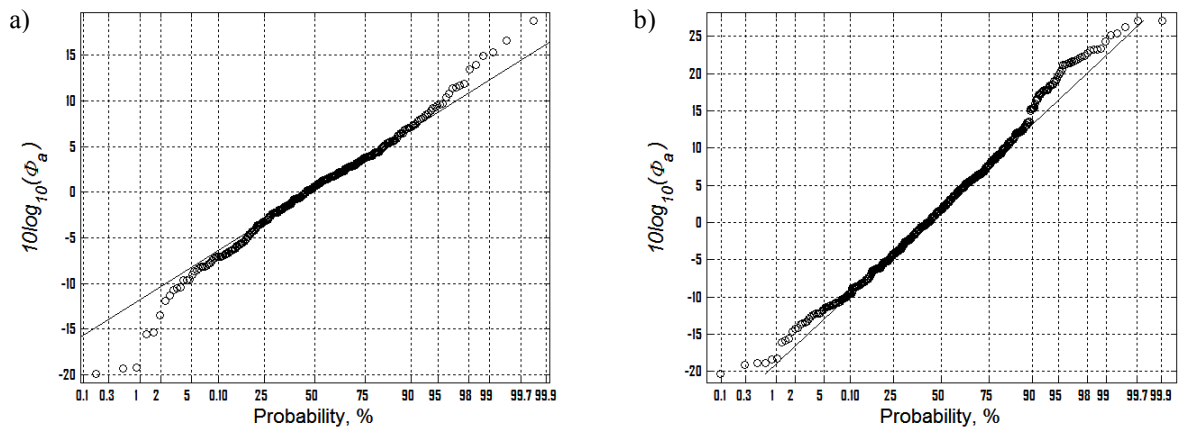


Fig. 15 Log-transformed initial methane fluxes from individual seeps in the shelf (a) and deep-sea (b) sectors shown on the normal quantile plots. The solid line represents a linear fit through the data points aggregated between 25% and 75% quartiles

Рис. 15 Индивидуальные начальные потоки сипов в шельфовом (а) и глубоководном (б) участках на графиках квантилей нормальной функции распределения. Линейная аппроксимация, оцененная по данным, сгруппированным между квантилями 25% и 75%, показана сплошной линией

Averaged over depth intervals the individual estimates of initial methane fluxes Φ_0 from 811 seeps are shown in Fig. 16.

It appeared unexpected for us that seep fluxes so dramatically trend towards an increase with the water depth increment as observed in Fig. 14. We have examined our data with due attention. Variation of bubble backscattering cross-sections

through a resonance effect was considered as the most probable cause of artifacts, resulting in increase of s_v values in (11) for deep seeps and, hence, overestimation of seep productivity N . Using formulae (A6.1.16) and (A6.1.21) from [19], we recomputed the aggregated echo return from the ensemble of bubbles, which size distribution corresponds to Fig. 6b.

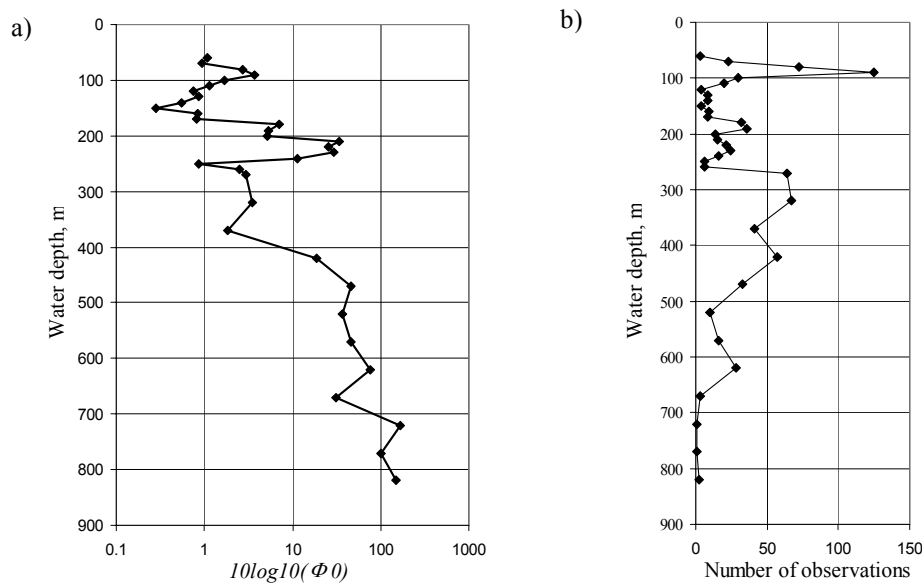


Fig. 16 Individual initial methane fluxes from 811 seeps, averaged over depth intervals (a); (b) – number of averaged observations

Рис. 16 Індивідуальні початкові потоки 811 сипов, усередненні по інтервалам глибин (а); (b) – обсяг даних при усередненні

In contrast to (15), these formulae allow estimating of the bubble acoustic properties depending on depth and a number of other factors. The typical vertical distributions of temperature, salinity and water density in the Black Sea were employed in our calculations; methane was assumed as the dominant bubble gas species, therefore the heat capacity ratio for methane $\gamma = 1.31$ was applied; the Q-factor of bubbles was defined by 10.2. It should be noted, that our calculations concerned solely with bubbles from a thin near-bottom layer. At mean initial rising speed of 25 cm/s (Fig. 9 – 11), bubble residence time in this layer does not exceed 10 – 15 s. According to our model data, bubbles insignificantly change in size over such a short period of time (even bubbles of the lowest size class shrink by no more than 0.2 – 0.3 mm). Nevertheless, we made two alternative calculations – for initial bubble sizes and reduced by 0.3 mm. The results of our calculations showed that in both cases the overall echo return from bubbles at seep “roots” very slightly increases with depth. Thus, when depth changed from 200 to 800 m, the seep echo strength increased in the

first and the second cases by 0.23 dB and 0.26 dB, correspondingly, i.e. by values comparable with the accuracy of echosounder calibration. It can also be suggested that real initial sizes of deep seep bubbles are somewhat smaller than those used in our calculations; however we consider the strong influence of resonance effect on our N estimates to be improbable, for all that. Meanwhile, while studying the methane budget in the Black Sea, authors of [40] apply a geochemical box model, which predicts a local maximum of methane input from seeps at 700 m water depth. The question about the origin of this maximum remains open in [40], but with a glance at data shown in Fig. 16 it might be supposed that seep methane source strengthening with depth can be a factor affecting the modern Black Sea methane distribution and budget.

Comparing estimates of Φ_0 against Φ_a we found, that most amount of bubbling methane coming to the water column, transforms into the dissolved gas phase. The ratio Φ_a / Φ_0 is the less the more seepage depth and bubble methane can

reach sea surface only from those seeps, which are located at depths shallower than 262 m (Fig. 17).

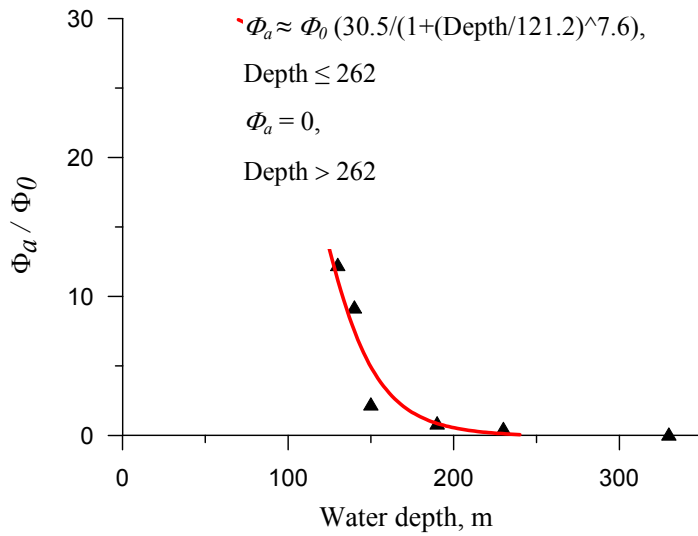


Fig. 17 Dependency of Φ_a / Φ_0 ratio on seep location depth (\blacktriangle). Solid line – an approximating curve. The approximate equation is shown.

Рис. 17 Зависимость Φ_a / Φ_0 от глубины расположения сипов (\blacktriangle). Сплошная линия – аппроксимирующая кривая. Приведено уравнение аппроксимации.

Statistical distributions of individual methane seep fluxes Φ_a (l/min STP) for both shallow and deep areas were also close to the log-normal law (рис. 18).

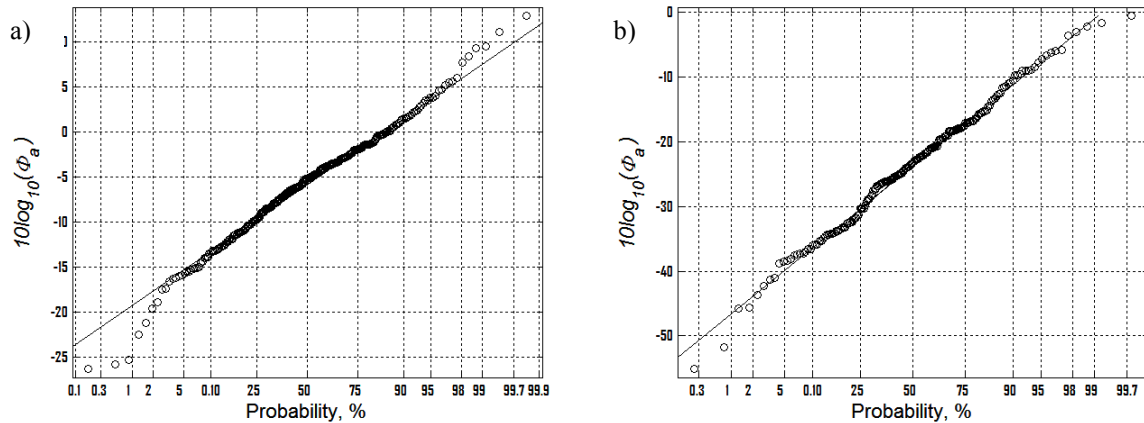


Fig. 18 Log-transformed individual methane fluxes to the atmosphere Φ_a from seeps in the shelf (a) and deep-sea (b) sectors shown on the normal quantile plots. The solid line represents a linear fit through the data points aggregated between 25% and 75% quartiles.

Рис. 18 Индивидуальные потоки метана в атмосферу Φ_a от сипов в шельфовом (а) и глубоководном (б) участках на графиках квантилей нормальной функции распределения. Линейная аппроксимация, оцененная по данным, сгруппированным между квантилями 25% и 75%, показана сплошной линией.

We made an assessment of individual methane fluxes Φ_0 and Φ_a for all detected in the investigated area 2200 seeps using the procedure as described below:

- a) seeps were ranked on location depth and distributed over the same depth intervals used for plotting Fig. 16a;
- b) the initial flux Φ_0 of those seeps, for which individual methane fluxes were not estimated di-

rectly, was equated to the mean value from the corresponding depth interval;

- c) fluxes Φ_a were calculated from initial fluxes Φ_0 according to the approximation equation Fig. 17.

The summary of obtained data over the whole investigated area is presented in Table 1, while the spatial distribution of seeps is shown in Fig. 19 and 20 where estimates of individual initial methane fluxes Φ_0 and fluxes to the atmosphere Φ_a are indicated.

Table 1 The summary of obtained data

Табл. 1 Суммарные данные наших исследований

Parameter	Sector A: depths 60 – 140 m	Sector B: depths 140 – 850 m
Acoustic coverage, km ²	41.2	345.9
Number of seeps	902	1298
Range of initial methane fluxes from individual seeps Φ_0 , l/min STP	0.01 – 74.91	0.01 – 509.82
Mean initial methane flux Φ_0 , l/min STP	2.47	22.86
Total initial methane flux Φ_0 , 10 ⁶ m ³ /year STP	1.17	15.57
Total methane flux to the atmosphere Φ_a , 10 ⁶ m ³ /year STP	0.31	0.01

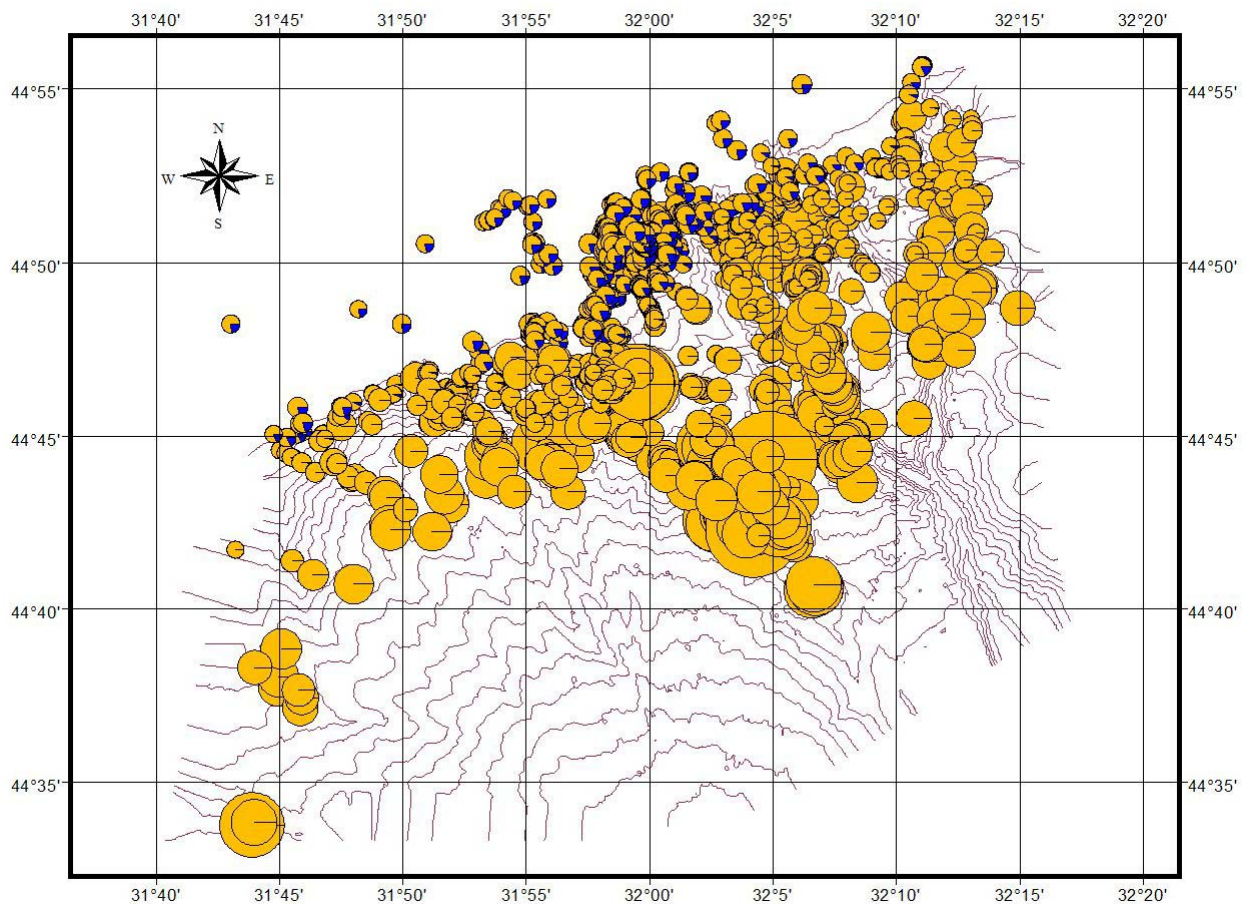


Fig. 19 Location map of observed seepages. Diameter of pie charts corresponds to the seep initial flux of methane Φ_0 . The least one matches 0.01 l/min STP, the largest - 509.82 l/min STP. Blue sectors in pie charts denote individual methane fluxes to the atmosphere Φ_a

Рис. 19 Пространственное распределение обнаруженных сипов. Диаметр круговых диаграмм отображает величину начального потока метана Φ_0 . Наименьший диаметр соответствует интервалу 0.01 л/мин STP, наибольший – 509.82 л/мин STP. Индивидуальные величины потока метана в атмосферу Φ_a обозначены на диаграммах секторами, закрашенными синим цветом

According to our estimates, 1387 or 63% of the total amount of seeps in the investigated

area deliver gaseous methane to the sea surface. However, the rate of atmospheric emission of

methane gas phase from seeps constitutes only 1.9% of the initial flux – $0.32 \cdot 10^6 \text{ m}^3 / \text{yr}$ or 0.23

$10^{-3} \text{ Tg} / \text{yr}$. Correspondingly, 98.1% of bubbling methane dissolves in the water column.

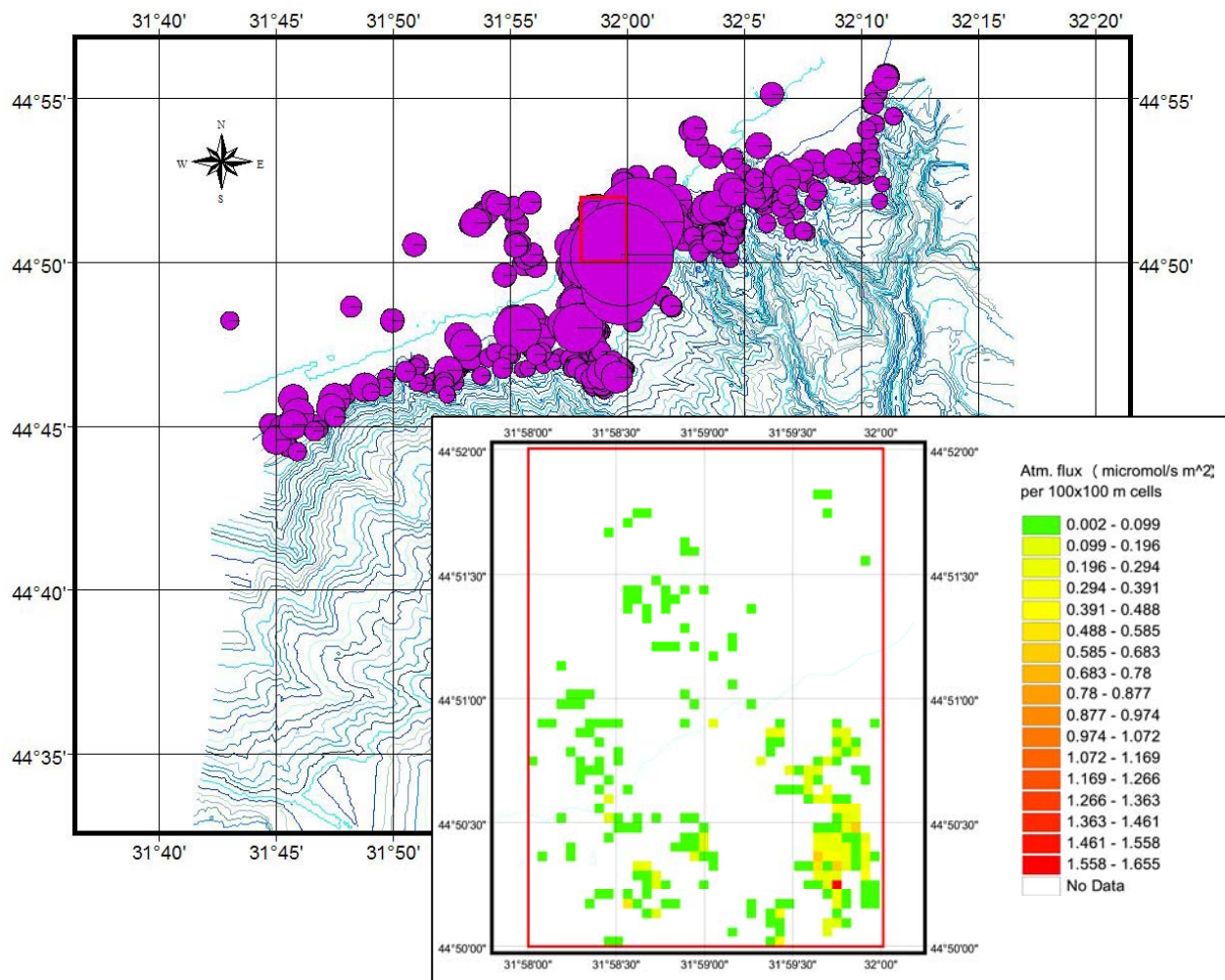


Fig. 20 Location map of observed seepages which emit methane gas phase to the atmosphere. Diameter of pie charts corresponds to the seep methane flux to the atmosphere Φ_a . The least diameter matches $3.13 \cdot 10^{-6} \text{ l/min STP}$, the largest – 19.46 l/min STP . The most intensive methane emanating area is shown in the inset, where averaged over $100 \times 100 \text{ m}$ cells Φ_a values are given

Рис. 20 Пространственное распределение сипов, эмитирующих газообразный метан в атмосферу. Диаметр круговых диаграмм отображает величину потока Φ_a . Наименьший диаметр соответствует $3.13 \cdot 10^{-6} \text{ л/мин STP}$, наибольший – 19.46 л/мин STP . На врезке – карта участка наиболее интенсивного газовыделения в атмосфере, где показанные значения Φ_a усреднены в ячейках $100 \times 100 \text{ м}$

Conclusions. To estimate methane flux from natural gas bubble streams (seepages) a combined approach is applied, inclusive of detailed echo survey of investigated area and data analysis with the use of specialized software, GIS technique and mathematic simulation.

A precise location map of methane seepages in the Dnieper paleo-delta region is obtained.

In total 2200 seepages have been identified at the investigated area of 387.1 km^2 , which release $16.74 \cdot 10^6 \text{ m}^3 \text{ STP}$, or $12.0 \cdot 10^{-3} \text{ Tg}$ of methane a year. Our data confirm the hypothesis about log-normal statistical distribution of methane fluxes from natural seeps, which is commonly utilized for regional flux estimations by extrapolation from

a few measurements of individual seepage rates as calibration points.

Our data evidence, that only 1.9% of the total amount of methane, released from gas seeps, reaches the atmosphere with bubbles. Thereby it is interesting to compare atmospheric emission rates of gaseous and dissolved methane from the sea surface. Data on the sea-air methane flux were acquired in the work [57], performed in the Dnieper paleo-delta in parallel with our survey during the 2003 CRIMEA cruise. The results of the methane flux calculations are reported in [57] separately for shelf (water depth < 200 m) and open waters (water depth > 200 m). Depending on calculation method, the mean emission rate from the shelf area was 0.32 – 0.77 nmol/m²s, while from open sea water 0.19 – 0.47 nmol/m²s [57]. Having divided our estimations for the total flux Φ_a from surveyed sectors A and B by their areas (Table 1), we determined that the area averaged

atmospheric flux of free seepage methane over sector A constitutes 3.6 nmol/m²s, one order of magnitude more than that of dissolved methane, while over sector B it decreases to 0.015 nmol/m²s, considerably less in comparison with dissolved methane phase. Consequently, taking into account the local character of seep spatial distribution (see insets in Fig. 1 and 20), the direct contribution of gas bubble streams to atmospheric emission of methane on the entire Black Sea basin seems to be insignificant. At the same time, most of seep methane remains in sea water, enters into physical, chemical and biological transformation processes of carbon-containing compounds and may play an important role in the Black Sea basin-wide methane budget.

Acknowledgements. This work was supported by the EU Project CRIMEA (Contract No. EVK2-2001-00322).

1. Геворкьян В. Х., Бураков В. И., Исагулова Ю. К. и др. Газовыделяющие постройки на дне северо-западной части Черного моря // Докл. АН УССР. – 1991. – № 4. – С. 80 – 85.
2. Егоров В.Н., Поликарпов Г.Г., Гулин М.Б., Артемьев Ю.Г., Стокозов Н. А., Гулин С.Б. Влияние струйных метановых газовыделений из дна Черного моря на мелкомасштабные процессы вертикального перемешивания вод // Доп. НАНУ. – 1999. – № 8. – С. 186 – 190.
3. В. Н. Егоров, Г. Г. Поликарпов, С. Б. Гулин, Ю. Г. Артемьев, Н. А. Стокозов, С. К. Костова. Современные представления о средообразующей и экологической роли струйных метановых газовыделений со дна черного моря. // Морск. экол. журн. - 2003. – 2, 3. – С. 5 – 26.
4. Иванов М. В., Поликарпов Г. Г., Леин А. Ю. и др. Биогеохимия цикла углерода в районе метановых газовыделений Черного моря // Докл. АН СССР. – 1991. – 3, № 5. – С. 1235 – 1240.
5. Леин А. Ю., Иванов М. В., Пименов Н. В. Генезис метана холодных метановых сипов днепровского каньона в Черном море // Докл. РАН. – 2002. – 387, № 2. – С. 242 – 244.
6. Поликарпов Г. Г., Егоров В. М. Виявлено активні газовиділення з дна Чорного моря // Вісн. АН УРСР. – 1989. – № 10. – С. 108 – 111.
7. Поликарпов Г. Г., Егоров В. Н., Нежданов А. И. и др. Явление активного газовыделения из поднятий на свале глубин западной части Черного моря // Докл. АН УССР. – 1989. – Сер. Б, № 12. – С. 13 – 15.
8. Поликарпов Г. Г., Егоров В. Н., Гулин С.Б. и др. Газовыделения со дна Черного моря - новый объект молисмологии // Молисмология Чёрного моря. – Киев: Наук. думка, 1992. – С. 5 – 10.
9. Поликарпов Г. Г., Иванов М. В., Гулин С. Б., Гулин М. Б. Депонирование углерода метана в карбонатных бактериальных постройках на свале глубин сероводородной зоны Черного моря // Докл. НАН Украины. – 1993. – № 7. – С. 93 – 94.
10. Шнюков Е. Ф., Соболевский Ю. В., Кутний В. А. Необычные карбонатные постройки континентального склона северо-западной части Черного моря – вероятное следствие дегазации недр // Литология и полезные ископаемые. – 1995. – № 5. – С. 541 – 561.
11. Шнюков Е. Ф., Пасынков А. А., Клещенко С. А. и др. Газовые факелы на дне Черного моря. - Киев, 1999. — 134 с.
12. Шнюков Е. Ф., Старостенко В. И., Гожик П. Ф. и др. О газоотдаче дна Черного моря // Геол. журн. – 2001. – С. 7 - 14.

13. Шнюков Е. Ф., Клещенко С. А., Артемов Ю. Г. Новое поле газовых факелов в западной части Черного моря // Геофиз. журн. – 2003. – № 2. – С. 153 - 160.
14. Alves S. S., Orvalho S. P., Vasconcelos J. M. T. Effect of bubble contamination on rise velocity and mass transfer // Chem. Eng. Sci. – 2005. – **60**. – P. 1 - 9.
15. Artemov, Yu. G. Software support for investigation of natural methane seeps by hydroacoustic method // Mar. Ecol. J. – 2006. – **5**, no. 1. – P. 57 - 71.
16. Artemov Yu. G. Modeling of natural methane bubbles in the Black Sea environment. (in prep).
17. Bodholt H. Variance error in echo integration output // Rapp. P.-v. Reun. Cons. perm. Int. Explor. Mer. – 1977. – **170**. – P. 196 - 204.
18. Clark J. F., Leifer I., Washburn L., Luyendyk B. Compositional changes in natural gas bubble plumes: observations from the Coal Oil Point marine hydrocarbon seep field // Geo-marine Letters. – 2004. – **23**. – P. 187 - 193.
19. Clay C.S., Medwin H. Acoustical oceanography: principles and applications // John Wiley & Sons, N. Y. – 1977. – 544 p.
20. Clift, R., Grace J. R., Weber M. E.. Bubbles, Drops, and Particles // Elsevier, N. Y. – 1978. – 380 p.
21. Cranston R.E. Marine sediments as a source of atmospheric methane // Bull. Geol. Soc. Denmark. – 1994. – **14**. – P. 101 - 109.
22. Cranston R.E, Ginsburg G.D, Soloviev V.A, Lorenson T.D. Gas venting and hydrate deposits in the Okhotsk Sea // Bull. Geol. Soc. Denmark. – 1994. – **41**. – P. 80 - 85.
23. Dando, P. R., Jensen P., O'Hara S. C. M. et al. The effects of methane seepage at an intertidal/shallow subtidal site on the shore of the Kattegat, Vendsyssel, Denmark // Bull. Geol. Soc. Denmark. – 1994. – **41**. – P. 65 - 79.
24. Dimitrov L. I. Characteristics of gas-acoustic anomalies on the South Bulgarian Black Sea shelf // Oceanology. – 1989. – **19**. – P. 34 - 41. (in Bulgarian).
25. Dimitrov L. Contribution to atmospheric methane by natural gas seepages on the Bulgarian continental shelf // Continental Shelf Researches. – 2002. – **22**. – P. 2429 - 2442.
26. Egorov V. N., Luth U., Luth C., Gulin M. B. Gas seeps in the submarine Dniepr paleo-delta, Black Sea: Acoustic, video and trawl data // Luth U., Luth C., Thiel H. Berichte aus den ZMK, Reihe E. – Hamburg: Hamburg University. – 1998. – **14**. – P. 11 - 22.
27. Foote K. G. Linearity of fisheries acoustics with addition theorems // J. Acoust. Soc. America. – 1983. – **73** (6). – P. 1932 - 1940.
28. Frumkin, A., Levich, V.G. On surfactants and interfacial motion // Zhurnal Fizicheskoi Khimii. – 1947. – **21**. – P. 1183 - 1204 (in Russian).
29. Gulin S.B., Polikarpov G.G., Egorov V.N. The age of microbial carbonate structures grown at methane seeps in the Black Sea with an implication of dating of the seeping methane // Marine Chemistry. – 2003. – **84**, no. 1 - 2. – P. 67 - 72.
30. Gulin S. B., Greinert J., Egorov V. N. et al. Observation of microbial carbonate build-ups growing at methane seeps near the upper boundary of the gas-hydrate stability zone in the Black Sea // Mar. Ecol. J. – 2005. – **4**, no. 3. – P. 5 - 14.
31. Hornafius J. S., Quigley D. C., Luyendyk B. P. The world's most spectacular marine hydrocarbons seeps (Coal Oil Point, Santa Barbara Channel, California): Quantification of emissions // J. Geophys. Res. – 1999. – **104**, C9. – P. 20703 - 20711.
32. Houghton J.T., Ding Y., Griggs D.J., Noguer M., et al. Climate Change 2001: The Scientific Basis // Contribution of Working Group I to the Third Assessment Report of the Intergovernmental Panel on Climate Change (IPCC). Cambridge University Press, Cambridge. – 2001. – 944 p.
33. Hovland M., Judd A.G. Seabed Pockmarks and Seepages: Impact on Geology, Biology and the Marine Environment // Graham & Trotman, London. – 1988. – 293 p.
34. Hovland M., Judd A.G., Burke R.A. The global production of methane from shallow submarine sources // Chemosphere. – 1993. – **26**. – P. 559 - 78.
35. Hunter K. A. Chemistry of the sea-surface microlayer. In The sea surface and global change (ed. L. P.S. and R. A. Duce). Cambridge Univ. Press, 1997.
36. Intergovernmental Panel on Climate Change Climate Change 2001—The Scientific Basis, 881 pp., Cambridge Univ. Press, New York, 2001. P. 775 – 778, doi:10.1038/44545.
37. Ivanov M.V., Pimenov N.V., Rusanov I.I., Lein A.Y. Microbial processes of the methane cycle at the north-western shelf of the Black Sea, Estuar. Coast. Shelf Sci. 54 (2002) 589–599.

38. Judd A.G., Davies G., Wilson J. et al. Contributions to atmospheric methane by natural seepages on the UK continental shelf // *Marine Geology*. – 1997. – **137**. – P. 165 - 189.
39. Judd A., Charlier R., Larox A., Lambert G., Rouland C. Minor sources of methane. Atmospheric Methane, Sources, Sinks and Role in the Global Change // NATO ASI Series, Series I: Global Environmental Change. – 1993. – **13**. – P. 432 - 456.
40. Kessler J.D., Reeburgh W.S., Southon J. et al. Basin-wide estimates of the input of methane from seeps and clathrates to the Black Sea // *Earth and Planetary Science Letters*. – 2006. – **243**. – P. 366 - 375.
41. Kvenvolden K.A., Lorenson T.D., Reeburgh W.S. Attention turns to naturally occurring methane seepage // *EOS (American Geophysical Union Transactions)*. – 2001. – **82**. – P. 457.
42. Leifer I., Patro R. K. The bubble mechanism for methane transport from the shallow sea bed to the surface: A review and sensitivity study // *Cont. Shelf Res.* – 2002. – **22**. – P. 2409 - 2428.
43. Levich V. G. *Physicochemical Hydrodynamics* // Prentice-Hall, Englewood Cliffs, NJ, 1962. – 591 p.
44. Lewis K., Marshall B. Seep faunas and other indicators of methane rich dewatering on New Zealand convergent margins // *N. Z. J. Geol. Geophys.* – 1996. – **39**. – P. 181 - 200.
45. Luth C., Luth U., Gebruk A.V., Thiel H. Methane gas seeps along the oxic/anoxic gradient in the Black Sea: manifestations, biogenic sediment compounds and preliminary results on benthic ecology // *Mar. Ecol.* – 1999. – **20**. – P. 221 - 249.
46. McGinnis D. F., Greinert J., Artemov Y. et al. Fate of rising methane bubbles in stratified waters: How much methane reaches the atmosphere? // *J. Geophys. Res.* – 2006. – **111**, no. C09007. – P. 1 - 15.
47. Merewether R., Olsson M. S., Lonsdale P. Acoustically detected hydrocarbon plumes rising from 2-km depths in Guaymas Basin, Gulf of California // *J. Geophys. Res.* – 1985. – **90**, no. 4. – P. 3075 - 3085.
48. Michaelis W., Seifert R., Nauhaus K. et al. Microbial reefs in the Black Sea fuelled by anaerobic oxidation of methane // *Science*. – 2002. – **297**. – P. 1013 - 1015.
49. Naudts L., Greinert J., Artemov Y. et al. Geological and morphological setting of 2778 methane seeps in the Dnepr paleo-delta, northwestern Black Sea // *Mar. Geol.* – 2006. – **227**. – P. 177 - 199.
50. Patro R., Leifer I., Bowyer P.. Better bubble process modeling : Improved bubble hydrodynamics parameterization // In: *Gas Transfer and Water Surfaces*, Eds. M. Donelan, W. Drennan, E.S. Salzman, and R. Wanninkhof, AGU Monograph. – 2001. – **127**. – P. 315 - 320.
51. Paull C. K., Ill W. U., Borowski W. S, Spiess F. N. Methanerich plumes on the Carolina continent rise associated with gas hydrates // *Geology*. – 1995. – **23**. – P. 89 - 92.
52. Prather, M., Derwent R., Ehhalt D. et al. Other trace gases and atmospheric chemistry // In: *Climate Change 1994: Radiative Forcing of Climate Change and an Evaluation of the IPCC IS92 Emission Scenarios*, edited by J. T. Houghton et al., Cambridge Univ. Press, New York. – 1995. – P. 73 - 126.
53. Quigley D.C. Quantifying spatial and temporal variations in the distribution of natural marine hydrocarbon seeps in the Santa Barbara Channel, California // Masters Thesis, Department of Geological Sciences. University of California, Santa Barbara, CA. – 1997. – P. 95.
54. Rowland F. S. Methane and chlorocarbons in the earth's atmosphere // *Origins Life*. – 1985. – **15**. – P. 279 - 297.
55. Reeburgh W. S. Global methane biogeochemistry // In: *The Atmosphere*, edited by R. Keeling, Elsevier, New York. – 2003. – P. 65 - 69.
56. Sadhal S. S., Johnson R. E. Stokes flow past bubbles and drops partially coated with thin films. Part 1. Stagnant cap of surfactant film – exact solution // *J. Fluid Mech.* – 1983. – **126**. – P. 237 - 250.
57. Schmale O., Greinert J., Rehder G.. Methane emission from high-intensity marine gas seeps in the Black Sea into the atmosphere // *Geophys. Res. Lett.* – 2005. – **32**, no. L07609. – P. 1 - 4.
58. Simoneit B.R.T., Lonsdale P.F., Edmond J.M., Shanks W.C. III, 1990: Deep-water hydrocarbon seeps in Guaymas Basin, Gulf of California. *Applied Geochemistry*, 5, 41-49.
59. Simrad (1992), Simrad EK500 Scientific Echo Sounder Instruction Manual, Simrad Subsea P2170, Horten, Norway.
60. Thome R. E. Investigations into the relation between integrated echo voltage and fish density // *Journal of the Fisheries Research Board of Canada*. – 1971. – **28**. – P. 1269 - 1273.

61. *Urick R. J.* Principles of underwater sound, 2nd edition. // New York, McGraw Hill. – 1975. – 384 p.
62. *Vasconcelos, J. M. T., Orvalho S. P., Alves S. S.* Gas-liquid mass transfer to single bubbles: Effect of surface contamination // *AIChE J.* – 2002. – **48**. – P. 1145 - 1154.
63. *Vasconcelos J. M. T., Rodrigues J. M. L., Orvalho S. C. P.* et al. Effect of contaminants on mass transfer coefficients in bubble column and airlift contactors // *Chem. Eng. Sci.* – 2003. – **58**. – P. 1431 - 1440.
64. *Washburn L., Clark J. F., Kyriakidis P.* The spatial scales, distribution, and intensity of natural marine hydrocarbon seeps near Coal Oil Point, California // *Mar. Pet. Geol.* – 2005. – **22**, no. 4. – P. 569 - 578.
65. *Wilson R.D., Monaghan P.H., Osanik A.* et al. Natural marine oil seepage // *Science.* – 1974. – **184**. – P. 857 - 865.
66. *Wüest A., Brooks N. H., Imboden D. M.* Bubble plume modeling for lake restoration // *Water Resour. Res.* – 1992. – **28**. – P. 3235 - 3250.
67. *Zheng L., Yapa P. D.* Modeling gas dissolution in deepwater oil/gas spills // *J. Mar. Syst.* – 2002. – **31**. – P. 299 - 309.
68. *Zimmermann S., Hughes R.G., Flügel H.J.* The effect of methane seepage on the spatial distribution of oxygen and dissolved sulphide within a muddy sediment // *Marine Geology.* – 1997. – **137**. – P. 149 - 157.

Поступила 12 марта 2007 г.

Емиссия метана в гидро - и атмосферу струйными газовыделениями в районе палео-дельты р. Днепр в Черном море. Ю. Г. Артемов, В. Н. Егоров, Г. Г. Поликарпов, С. Б. Гулин. Для оценки потока метана от струйных газовыделений (сипов) применен комбинированный подход, включающий проведение детальной акустической съемки исследуемого района и анализ данных с использованием специализированного программного обеспечения, технологии ГИС и методов математического моделирования. Получена подробная карта распределения метановых сипов в районе палео-русла р. Днепр. Всего на площади 387.1 км², обследованной в этом районе, идентифицировано 2200 сипов, выделяющих 16.7 10⁶ м³ при атмосферном давлении (STP), или 12.0 10⁻³ тераграмм (Тг) метана в год. Статистическое распределение индивидуальных потоков метана от сипов соответствует логнормальному закону. По нашим оценкам, 1.9 % метана струйных газовыделений достигает атмосферы в газообразном состоянии, а 98.1% растворяется в водном столбе. Таким образом, подавляющая часть метана остается в морской воде и включается в физические, химические и биологические процессы трансформации углеродсодержащих соединений.

Ключевые слова: Черное море, палео-русло р. Днепр, струйные метановые газовыделения, поток метана.

Емісія метану в гідро - і атмосферу струминними виходами газу у районі палео-дельти р. Дніпр у Чорному морі. Ю. Г. Артемов, В. М. Єгоров, Г. Г. Полікарпов, С. Б. Гулін. Для оцінювання потоку метану від струминних виходів газу (сипів) був застосований комбінований підхід, включаючий здійснення докладної акустичної зйомки досліджуваного району й аналіз даних з використанням спеціалізованого програмного забезпечення, технології ГІС і методів математичного моделювання. Отримана докладна мапа розподілу метанових сипів у районі палео-русла р. Дніпр. Разом на площі 387.1 км², обстеженої у цьому районі, ідентифіковано 2200 сипів, виділяючих 16.7 10⁶ м³ при атмосферному тиску (STP), або 12.0 10⁻³ тераграм (Тг) метану щорічно. Статистичний розподіл індивідуальних потоків метану від сипів відповідає логнормальному закону. За нашими оцінками, 1.9 % метану струминних виходів газу досягають атмосфери у газоподібному стані, але 98.1% розчиняються у водному стовпі. Таким чином, переважна частина метану залишається у морській воді та включається у фізичні, хімічні і біологічні процеси трансформації вугле-містячих сполук.

Ключові слова: Чорне море, палео-русло р. Дніпр, струминні виходи метану, потік метану.